


## Adiabaticity parameters for the categorization of light-matter interaction: From weak to strong driving

Christian Heide<sup>⊗,\*†</sup>, Tobias Boolakee<sup>⊗,\*‡</sup>, Takuya Higuchi, and Peter Hommelhoff<sup>⊗§</sup>  
*Laser Physics, Department of Physics, Friedrich-Alexander-Universität Erlangen-Nürnberg (FAU),  
 Staudtstrasse 1, D-91058 Erlangen, Germany*

 (Received 2 July 2020; accepted 16 July 2021; published 13 August 2021)

We investigate theoretically and numerically the light-matter interaction in a two-band system (TBS) as a model system for excitation in a solid-state band structure. We identify five clearly distinct excitation regimes, categorized with well-known adiabaticity parameters: (1) the perturbative multiphoton absorption regime for small driving field strengths, and four light-field-driven regimes, where intraband motion becomes important (2) the impulsive Landau-Zener (LZ) regime, (3) the nonimpulsive LZ regime, (4) the adiabatic regime, and (5) the adiabatic-impulsive regime for large electric field strengths. This categorization is tremendously helpful to understand the highly complex excitation dynamics in solids, in particular, when the driving field strength varies, and this categorization naturally connects Rabi physics with Landau-Zener physics. In addition, we find an insightful analytical expression for the photon orders connecting the perturbative multiphoton regime with the light-field-driven regimes. Moreover, in the adiabatic-impulsive regime, adiabatic motion and impulsive LZ transitions are equally important, leading to a broken symmetry of the TBS and a residual current when applying few-cycle laser pulses of broken temporal symmetry. This categorization allows a deep understanding of strong-field excitation in solids, including current and high-harmonic generation in a large variety of settings, and will help to find optimal driving parameters for a given purpose.

DOI: [10.1103/PhysRevA.104.023103](https://doi.org/10.1103/PhysRevA.104.023103)

### I. INTRODUCTION

The understanding of the interaction of intense optical fields with atoms or solids has facilitated controlling electrons coherently on ultrashort timescales. This gave rise to new research areas including the efficient generation of high-harmonics [1–4], light-field-driven ionization and electron emission [5], and light-field-driven current generation in solids [6–8]. More recently, coherent electron dynamics has been investigated in two-dimensional [9–15] and topologically relevant [16–22] materials. In all these cases, the underlying physics can often be simplified, categorized, and described with a two-band system (TBS) interacting with light. Here, we provide a clear categorization of different excitation regimes using well-known adiabaticity parameters, with a focus on solids.

As long as the light-field is weak, momentum exchange between light and electrons, i.e., intraband motion, can be neglected, and the occupation of the bands is well described by resonant Rabi physics, with interband transitions only [13,23–25]. This picture, however, becomes unsuited or at least difficult to interpret when the light field becomes so strong that the light field changes the momentum of the electrons, causing intraband motion within their respective bands. In this

case, the electron dynamics is better described as (repeated) Landau-Zener transitions, between valence and conduction bands [6–8,25–34]. A sufficient basis to describe intraband motion and interband transitions is the Houston basis [8,31].

Whereas pure nonadiabatic interband or adiabatic intraband electron dynamics have been well investigated in the context of strong-field physics, such as with high-harmonic generation (HHG) in solids [1–3,9,16,32,35–39], intraband motion and interband transitions acting in a combined fashion have been investigated to a less comprehensive degree. Based on adiabaticity parameters, we identify a regime of light-matter interaction, where both intraband motion and interband transitions generate an off-resonant, residual excitation. In contrast to HHG, which is not able to probe this off-resonant excitation directly, it can be well observed as a residual current [7,8,10]. With this regime, we can now give a complete and a general picture of TBS physics and can categorize it into five clearly distinct regimes.

In his seminal paper, Keldysh introduced the adiabaticity parameter  $\gamma \equiv \omega\sqrt{m^*}\Delta/(eE_0)$  for electrons in a TBS [40]. Here,  $\omega$  is the driving frequency of the light,  $E_0$  its peak electric field strength,  $m^*$  the effective electron mass,  $\Delta$  the band gap, and  $e$  the electron charge. Assuming monochromatic light and excitation around the band gap, we can express the Keldysh parameter as

$$\gamma = \frac{\Delta\hbar\omega}{2\hbar v_F e E_0} = \frac{\Delta}{2\hbar\Omega_R}, \quad (1)$$

\*These authors contributed equally to this work.

†christian.heide@fau.de

‡tobias.boolakee@fau.de

§peter.hommelhoff@fau.de

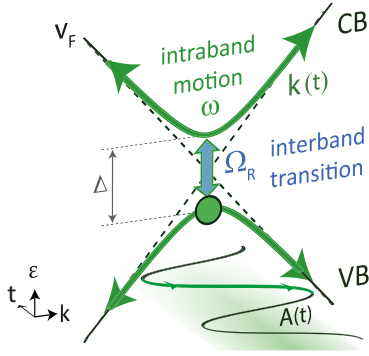


FIG. 1. Light-field-driven electron dynamics in a two-band system. The valence (VB) and the conduction band (CB) are separated by a band gap  $\Delta$  and have asymptotic slopes defining the Fermi velocity  $v_F$ . When the electric field is small, intraband motion can be neglected and the excitation oscillates resonantly between the bands with the Rabi frequency  $\Omega_R$ . When the electric field becomes strong, the Rabi frequency exceeds the driving frequency, and intraband motion strongly influences interband transitions.

with  $\Omega_R = v_F e E_0 / (\hbar \omega)$  being the Rabi frequency and  $v_F$  the Fermi velocity (see Fig. 1 and the Appendix for a detailed derivation). When  $2\hbar\Omega_R$  exceeds  $\Delta$ ,  $\gamma$  becomes smaller than 1 and the light-matter interaction enters the well-known strong-field regime.

In the case of resonant excitation,  $\Delta = \hbar\omega$ , we obtain the resonant adiabaticity parameter from Eq. (1) [31,41,42] as

$$z_{\mathcal{R}} = \frac{2\Omega_R}{\omega}. \quad (2)$$

Here,  $2\Omega_R$  can be interpreted as the inverse of the transition time  $\tau_t$  [ $2\Omega_R = (2\pi)/\tau_t$ ] from the valence to the conduction band. Figure 1 shows schematically the competition of Rabi oscillations with  $\Omega_R$  (blue arrow) and intraband motion, driven with  $\omega$  (thick green arrows). When  $\tau_t$  becomes shorter than the driving period of the light,  $z_{\mathcal{R}}$  becomes larger than 1. In that regime, colloquially speaking, the electron has enough time to undergo a transition from one to the other band within an optical cycle.

## II. MODEL SIMULATIONS

We continue with further insightful parameters later but now first model the light-matter interaction by solving the time-dependent Schrödinger equation numerically [7,8]. For the simulation we apply the following approximations: (i) We treat the light-matter interaction semiclassically, (ii) we utilize the electric dipole approximation, (iii) we limit our discussion to two bands, i.e., the valence and conduction band, (iv) we assume that the electron dynamics can be represented by an evolution of field-free Bloch states, and (v) we assume that the electrons can be treated independently during the light-matter interaction. We note that these approximations are commonly applied in the strong-field community to describe high-harmonic generation or the residual conduction band population. These approximations allow us to obtain a simple and intuitive classification of light-matter interaction in solids.

We consider a TBS with a band gap of  $\pm\Delta/2$  and a time-dependent perturbation  $\alpha(t)/2$ , representing an avoided crossing [26,28,43–45]. The Hamiltonian of this system reads as follows:

$$\hat{\mathcal{H}}(t) = -\frac{\alpha(t)}{2}\hat{\sigma}_x - \frac{\Delta}{2}\hat{\sigma}_z, \quad (3)$$

with  $\hat{\sigma}_x$  and  $\hat{\sigma}_z$  being the Pauli matrices. The eigenenergies are  $\varepsilon_{\pm}(t) \equiv \pm\frac{1}{2}\varepsilon(t)$ , where  $\varepsilon(t) = \sqrt{\Delta^2 + \alpha(t)^2}$  is the time-dependent energy difference between the two bands. By taking  $k(t)$  as the time-dependent wave number of an electron and  $\pm v_F$  as the slopes of the two crossing bands, Eq. (3) with  $\alpha(t) = 2\hbar v_F k(t)$  represents a solid-state band structure with  $\varepsilon_{\pm}(k)$  being the conduction band (+) and valence band (−) energy (and  $\Delta$  being the band gap). We assume  $v_F = 1$  nm/fs. The change of the electron wave number due to the electric field is described by the Bloch acceleration theorem  $\dot{k}(t) = -(e/\hbar)E(t)$  [7,8,46,47]. We note that when the electric field is weak, the electron dynamics is well described with a trivial two-level system of fixed energy levels  $\varepsilon_{\pm}$  at each  $k$ -value, i.e., intraband motion can be neglected. However, when the electric field becomes large, the electrons undergo intraband motion. For even larger electric field strengths (i.e.,  $\gamma < 0.01$ ), relativistic effects may become important, which are beyond the presented categorization (see the Appendix).

In the simulations we apply a linearly polarized vector potential,

$$A(t) = -E_0/\omega \exp[-2 \ln 2(t/\tau_p)^2] \sin(\omega t + \phi_{\text{CEP}}), \quad (4)$$

associated with the electric field  $E(t) = -\dot{A}(t)$ , to model the temporal evolution of the conduction band population. By defining the vector potential we satisfy  $A(-\infty) = A(\infty)$  and thus omit dc components in the electric field. A pulse duration of  $\tau_p = 5$  fs is chosen with a central photon energy of  $\hbar\omega = 1.55$  eV and a carrier-envelope phase of  $\phi_{\text{CEP}} = \pi/2$ . For simplicity, we first consider electrons with an initial wave number of  $k_0 = 0$ . We note that while different pulse durations, dephasing or dispersion effects may change the population distribution, the presented categorization remains valid (see the Appendix).

## III. CATEGORIZATION OF LIGHT-MATTER INTERACTION

Figures 2(a)–2(e) show in the lower panels the conduction band population  $\rho^{\text{CB}}$  as a function of time for various regimes, discussed in detail in what follows. In Fig. 2(f), we show the residual conduction band population parametrized by  $\gamma$  and the multiphoton parameter  $M = \Delta/(\hbar\omega)$ , measuring the band gap in units of the photon energy. Based on  $\gamma$  and  $z_{\mathcal{R}}$  we can now identify and categorize various regimes, which show an entirely different temporal evolution of the conduction band population [Figs. 2(a)–2(e)].

(1) *Perturbative multiphoton absorption regime.* When the electric field is weak ( $\gamma > 1$ ), the population is found at  $M \approx 1$ , reflecting resonant excitation [Figs. 2(f) and 2(g)]. Here, the population  $\rho^{\text{CB}}$  rises during the laser pulse gradually [Fig. 2(a)]. The red lines, horizontal for  $\gamma > 1$ , represent the resonance condition:  $M$  is an integer. The population width along  $M$  reflects the spectral width of the laser pulse.

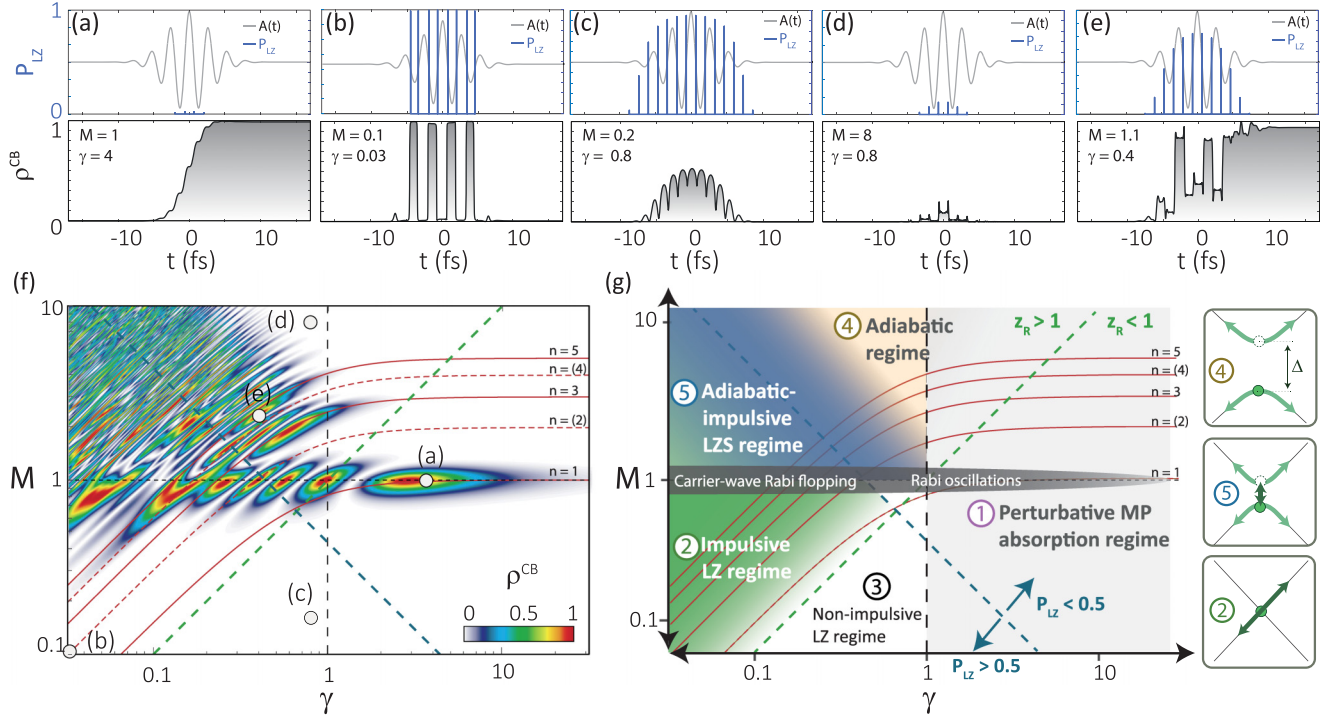


FIG. 2. Regimes of a light-field-driven two-band system. (a)–(e) Temporal evolution of the conduction band population  $\rho^{CB}$  for a Gaussian pulse ( $\tau_p = 5$  fs,  $\phi_{CEP} = \pi/2$ ) with electrons starting from  $k_0 = 0$  from our time-dependent Schrödinger equation (TDSE) model. The top panels show the normalized vector potential  $A(t)$  (gray lines) and  $P_{LZ}$  (blue lines) for an LZ transition at  $k_0$ . The laser and system parameters are identified by  $\gamma$  and  $M$ , given in each legend. (f) Map of the residual conduction band population. The circles relate to panels (a)–(e). See text for details. Panel (g) is the same as panel (f), with various regimes indicated: (1) Perturbative MP absorption regime, (2) impulsive LZ regime, (3) nonimpulsive LZ regime, (4) adiabatic regime, and (5) adiabatic-impulsive regime. Whereas for  $\gamma > 1$  only perturbative, resonant one-photon ( $n = 1$ ) absorption at  $M = 1$  is found, for  $\gamma < 1$  off-resonant excitation occurs. In particular, for  $P_{LZ} \approx 0.5$ ,  $\delta_{LZ} \approx \ln(2)/(2\pi)$ , and  $z_R > 1$ , defining the adiabatic-impulsive regime (5), most off-resonant excitation is found. The red lines represent odd (solid lines) and even (dashed lines) resonances for the light-matter interaction, based on Eq. (6). The boxes relate to three regimes as indicated by the number. Note the dashed lines showing the crossing areas for the various adiabaticity parameters.

Increasing the electric field strength (decreasing  $\gamma$ ) results in an increase of  $\Omega_R \propto E_0$ ; hence, Rabi oscillations become visible.

*Transition to the strong-field regime (2)–(5).* Around  $\gamma \approx 1$ , the interaction strength  $2\hbar\Omega_R$  is of the order of the band gap [Eq. (1)] and light-field-driven intraband motion cannot be neglected anymore. Hence, intraband motion leads to a variation of the instantaneous eigenenergies  $\varepsilon(t)$ , which in turn results in a rotation of the features in Fig. 2(f). For  $\gamma < 1$ , carrier-wave Rabi flopping occurs and the horizontal lines given by multiples of the photon energy fail as a valid quantity to specify resonant absorption, reflecting the ac Stark effect [25]. To extend the resonance condition to this field-driven regime, we calculate the dynamical phase

$$\phi = \frac{1}{\hbar} \int \varepsilon(t) dt. \quad (5)$$

When a phase of  $\phi = 2\pi$  is accumulated within an optical cycle of the laser pulse, population at the next higher multiphoton resonance ( $n$ ) is found [25]. For monochromatic excitation, we analytically obtain the resonance condition

$$M = \frac{n\pi}{2\varepsilon_l(-\gamma^{-2})}. \quad (6)$$

Here,  $\varepsilon_l$  denotes the complete elliptic integral of the second kind and  $n$  is the order of the resonance (see the Appendix). We see that when  $\gamma$  decreases, the photon resonances  $n$  no longer match integer multiples of  $M$  but are shifted towards smaller  $M$ . Equation (6) is plotted as red solid lines in Fig. 2(f), for various  $n$ , perfectly matching the conduction band population obtained from the TDSE simulation. When  $\gamma \gg 1$ , the elliptic integral becomes  $\pi/2$  and the photon resonances are found at integer multiples of the band gap, i.e.,  $M = n$ , as expected for weak fields. In contrast, at  $\gamma \approx 0.4$  the intraband motion becomes so strong that  $n = 2M$  and, thus, the two-photon resonance is found at  $M = 1$ . We note that due to the inversion symmetry of the TBS at  $k_0 = 0$  the population only arises for odd photon orders [see dashed lines for even orders in Fig. 2(f)].

In the field-driven regime, i.e.,  $\gamma < 1$ , it is helpful to describe the electron dynamics within the Landau-Zener (LZ) formalism (see the Appendix and Refs. [26,28,29,48,49]). When the electron reaches the minimal separation of valence and conduction bands, the transition from one to the other band takes the form of an LZ transition. The transition probability is approximated by the famous Landau-Zener formula

$$P_{LZ} = \exp(-2\pi\delta_{LZ}), \quad (7)$$

with

$$\delta_{\text{LZ}} = \frac{\Delta^2}{8\hbar^2\Omega_{\text{R}}\omega} = \frac{1}{4}\gamma\left(\frac{\hbar\omega}{\Delta}\right)^{-1} \quad (8)$$

being the Landau-Zener adiabaticity parameter (see the Appendix for derivation) [8,28,43,44].

Within the field-driven regime we now find four categories of electron dynamics.

(2) *Impulsive Landau-Zener regime.* When  $\delta_{\text{LZ}} \ll 1$  and  $z_{\text{R}} > 1$  the electron undergoes a sequence of fast LZ transitions with probability  $P_{\text{LZ}}$  close to unity [Fig. 2(b)]. Within one optical cycle the electron experiences a transition from the valence band to the conduction band and back to the valence band. After the laser pulse, the electron ends up in the initial band; hence, no excitation is found [Figs. 2(f) and 2(g)].

(3) *Nonimpulsive Landau-Zener regime.* When the transition time  $\tau_i$  is longer than the optical period (i.e.,  $z_{\text{R}} < 1$ ), the LZ transition can no longer be considered impulsive. Figure 2(c) shows that even when the LZ probability is large (blue lines in top panel) there is not enough time for an efficient electron excitation. Also, here, the conduction band is not populated after the laser pulse is gone, albeit for very different reasons than in the impulsive LZ regime [Fig. 2(f)].

(4) *Adiabatic regime.* When  $\delta_{\text{LZ}} \gg 1$ , the probability for an electron to undergo an LZ transition approaches zero and, thus, the electron undergoes pure intraband motion [Fig. 2(d)]. Yet, we note that the intraband motion during the laser pulse is a well-investigated source of intraband HHG [36,50].

(5) *Adiabatic-impulsive Landau-Zener-Stückelberg regime.* When  $\delta_{\text{LZ}} \approx \ln(2)/(2\pi)$ ,  $P_{\text{LZ}} \approx 0.5$ . Hence after one LZ transition event, the electron wave function is equally split into the valence and the conduction band, so a part of the electron wave function undergoes an LZ transition, while the remainder stays adiabatically in the valence band [Fig. 2(e)]. Due to the oscillatory nature of the driving, this happens periodically with every half cycle of the laser pulse. Interference of the electronic wave-function components, each with a different accumulated phase  $\phi$  [Eq. (5)], determines the conduction band excitation probability. We observe that, intriguingly, the net excitation probability is highest in this regime. We note that repeated coherent LZ transitions are called Landau-Zener-Stückelberg interference [26,28,43–45].

#### IV. RESIDUAL CURRENT IN A TWO-BAND SYSTEM

So far, we have discussed electrons starting from  $k_0 = 0$  only and described the light-field-driven electron dynamics. To capture the full excitation in the TBS and finally define a residual current, various initial  $k_0$  values throughout the two bands need to be taken into account. For linearly polarized light, we can focus on a one-dimensional band structure. Electrons with  $k_0 > 0$  and  $k_0 < 0$  can experience different dynamics, in particular, when a pulse with a broken time inversion symmetry [ $E(-t) \neq E(t)$ ] is applied, e.g., one with  $\phi_{\text{CEP}} = \pm\pi/2$  [8,14,15,33,51,52]. Figure 3(a) shows schematically the electron trajectory in reciprocal space for an electron starting at  $k_0 > 0$  (green line) and  $k_0 < 0$  (blue line). For  $\phi_{\text{CEP}} = \pm\pi/2$ , the number of LZ transitions and their temporal spacing between an electron starting at initially positive or negative wave number may differ, resulting in

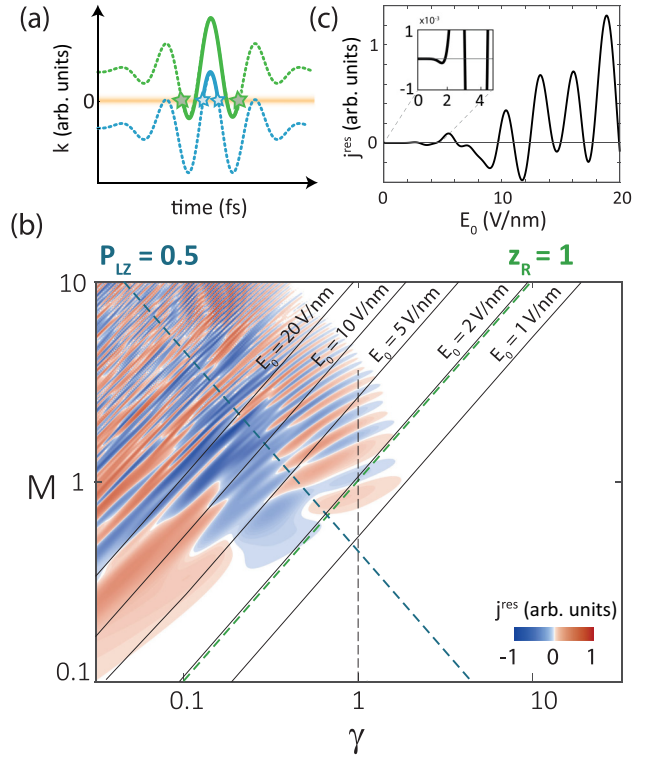


FIG. 3. (a) Temporal evolution of the electron trajectory for an electron with initially positive (green line) and negative (blue line) wave number. The orange line indicates the region of high LZ transition probability. For a field wave form with broken time inversion symmetry, the two electron trajectories can experience a different number of LZ transitions and/or a different total quantum-mechanical phase evolution, in particular, when the length of the trajectory (green and blue lines) is different. (b) Residual electric current as function of  $\gamma$  and  $M$  calculated with the TDSE model. The maximal residual current is found in the adiabatic-impulsive LZS regime. The black lines indicate iso-lines for constant  $E_0$ . (c) Integrated current along lines with constant  $E_0$ , as a function of  $E_0$ . The oscillatory nature of  $j^{\text{res}}(E_0)$  is a result of the wave-number-dependent quantum-mechanical phase evolution.

asymmetric residual population. As a consequence, a nonzero residual ballistic current,

$$j^{\text{res}} = g_s e \sum_{m=\text{CB,VB}} \int_{-\infty}^{\infty} v^{(m)}[k(t)] \rho^{(m)}(k_0, t) \frac{dk}{2\pi}, \quad (9)$$

with  $v^{(m)}(k) = \hbar^{-1} \frac{\partial \varepsilon_{\pm}(k)}{\partial k}$ , is generated. The factor  $g_s = 2$  accounts for two kinds of spins.

In Fig. 3(b) we show the map of the residual current density, taking all initial  $k_0$  values into account. With the help of the above, we can now understand the intricate pattern of the current map. Residual current is mainly found in the adiabatic-impulsive LZS regime. Increasing the electric field strength, i.e., decreasing  $\gamma$ , starting at  $\gamma \approx 1$ , results in an increase of the accumulated dynamical phase, causing more and more current reversals as a function of  $E_0$ . Iso-lines for constant electric field strengths  $E_0 = 1, \dots, 20$  V/nm are drawn as solid black lines. Around  $E_0 = 1$  V/nm almost no residual current is obtained. Increasing the electric field strength towards

2 V/nm results in nonzero  $j^{\text{res}}$ , at around 2 V/nm. This is shown and continued in the integrated current, along constant field strength in Fig. 3(c). The oscillatory nature of the current as a function of the electric field strength reflects Landau-Zener-Stückelberg interference with varying accumulated phase, as also discussed above. We note that the simulation results presented were obtained for a photon energy of 1.55 eV ( $\omega = 2\pi \cdot 0.375$  PHz). A smaller driving frequency  $\omega$  decreases the field strength required to enter the light-field controlled regimes, see Eqs. (1) and (2) and thus, the Landau-Zener-Stückelberg interferences are expected to appear at smaller field strengths.

### V. ANALOGY TO ATOMIC AND WIDE BAND-GAP SYSTEMS

In many light-matter interactions, the transition from the weak-field regime to the strong-field regime has been observed. This transition is typically identified by  $\gamma$  and  $z_{\mathcal{R}}$ , i.e., the ratio between the *interaction strength* and the *band gap* or the *photon energy*, respectively. For example, for atomic systems, the magnitude of the interaction strength is well described by the ponderomotive energy [40], while for wide band-gap solids, it is rather described by the Bloch frequency [31,53]. In the case of resonant and near-resonant excitation in a semiconductor, we find that the interaction strength can be well described in the form of an effective Rabi frequency. Based on our extensive analysis, we find that here  $\Omega_{\mathcal{R}}$  exceeds the photon energy at around 1.8 V/nm ( $z_{\mathcal{R}} > 1$ ). This also matches an important previous result: In Ref. [8] it was shown that the CEP-dependent photocurrent in graphene ( $v_F = 1$  V/nm) switches sign at a field strength of 1.8 V/nm, perfectly coinciding with the first current reversal shown in Fig. 3(c). Hence, the adiabatic-impulsive LZS regime has been entered in that experiment.

### VI. SUMMARY

In summary, we have presented five different regimes of light-matter interaction in a two-band system, categorized by adiabaticity parameters. This way, we can understand the intricate dynamics of each regime by delimiting it from but also connecting it to its neighboring regimes. Although we have focused on electrons in a solid-state band structure, the here-discussed dynamics and categorization into different regimes may be applicable to a large variety of two-band systems, which may include or give rise to nonadiabatic multielectron dynamics [49,54], conical intersections [55,56], Wannier-Stark localization [6,57], cavity QED [58,59], and the Kibble-Zurek mechanism [60] based on an effective TBS, for which the time-dependent perturbation  $\alpha(t)$  needs to be adapted appropriately. Specifically, two-dimensional materials can be well approximated as two-band systems [8,34,61,62]. We expect that the presented categorization will help us to understand fundamental yet complex light-matter interaction results on a new level across a large variety of solid-state systems.

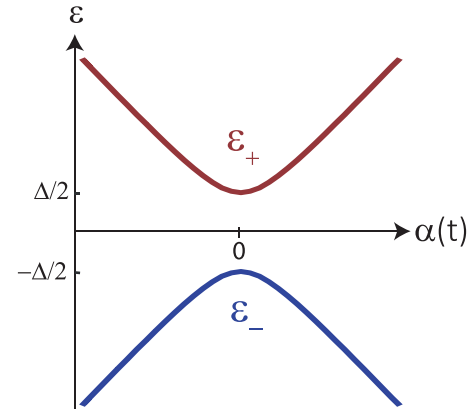


FIG. 4. Two-level system. Energy  $\varepsilon$  versus time-dependent energy bias  $\alpha$ . The blue and red solid lines represent the adiabatic energy basis of the two-level system with two instantaneous eigenstates  $\varepsilon_+$  and  $\varepsilon_-$ . For  $\alpha = 0$ , the energy difference  $\varepsilon(t)$  between the two eigenstates is given by  $\Delta$ .

### ACKNOWLEDGMENTS

We thank Vladislav S. Yakovlev for discussions. This work has been supported in part by the European Research Council (Consolidator Grant NearFieldAtto), the Deutsche Forschungsgemeinschaft (Sonderforschungsbereich 953 Synthetic Carbon Allotropes Project No. 182849149), and the PETACom project financed by the Future and Emerging Technologies Open H2020 program. C.H. acknowledges support from the Max Planck School of Photonics supported by BMBF. P.H. gratefully acknowledges a Fellowship from the Max Planck Institute for the Science of Light (MPL).

### APPENDIX

#### 1. General form of a two-level system

We consider a two-level system with two constant energy levels,  $\pm\Delta/2$ , and a time-dependent energy perturbation,  $\alpha(t)/2$ , acting on them, i.e., time-dependent coupling between energy levels. Such a system is described by the Hamiltonian

$$\hat{\mathcal{H}}(t) = \hat{\mathcal{H}}_0 + \hat{\mathcal{H}}_{\text{int}}(t) = -\frac{1}{2} \begin{pmatrix} \Delta & \alpha(t) \\ \alpha(t) & -\Delta \end{pmatrix}. \quad (\text{A1})$$

Here,  $\hat{\mathcal{H}}_0 = -\frac{\Delta}{2}\hat{\sigma}_z$  represents the bare two-level system with the two eigenvalues  $\pm\Delta/2$  and  $\hat{\mathcal{H}}_{\text{int}}(t) = -\frac{\alpha(t)}{2}\hat{\sigma}_x$  (the interaction Hamiltonian), describing how the system evolves under a time-dependent perturbation.  $\hat{\sigma}_x$  and  $\hat{\sigma}_z$  are Pauli matrices. By diagonalizing  $\hat{\mathcal{H}}(t)$ , one obtains the instantaneous eigenvalues

$$\varepsilon_{\pm}(t) \equiv \pm\frac{1}{2}\sqrt{\Delta^2 + \alpha(t)^2} = \pm\frac{1}{2}\varepsilon(t). \quad (\text{A2})$$

Hereby,

$$\varepsilon(t) = \sqrt{\Delta^2 + \alpha(t)^2} \quad (\text{A3})$$

is the time-dependent energy difference between the two energy states  $\varepsilon_+$  and  $\varepsilon_-$ , as depicted in Fig. 4.

## 2. Solid-state two-band model

One example of a TBS system can be found in the dynamics of an electron driven in a solid by an external field. By taking the Bloch acceleration theorem

$$k(t) = k_0 - \frac{e}{\hbar} \int E(t) dt, \quad (\text{A4})$$

as the time-dependent electron wave number, where  $A(t)$  is the vector potential and  $k_0$  the initial electron wave number, and

$$\alpha(t) = 2\hbar v_F k(t) \quad (\text{A5})$$

as the time-dependent energy bias, with  $v_F$  being the Fermi velocity, we can rewrite Eq. (A1) as

$$\hat{\mathcal{H}}(t) = \begin{pmatrix} -\frac{\Delta}{2} & \hbar v_F k(t) \\ \hbar v_F k(t) & \frac{\Delta}{2} \end{pmatrix}. \quad (\text{A6})$$

For  $k_0 = 0$  and the periodic oscillating electric field  $E(t) = E_0 \sin(\omega t)$ , Eq. (A6) has the form of that of a driven two-band Rabi system with

$$\Omega_R = \frac{v_F e E_0}{\hbar \omega} \quad (\text{A7})$$

being the Rabi frequency.  $\omega$  is the angular frequency and  $E_0$  the peak electric field strength.

To obtain the temporal evolution of an electron in the two-band model, we assume that the electron dynamics is coherent and can thus be described by the time-dependent Schrödinger equation

$$i\hbar \frac{\partial \Psi(k_0, t)}{\partial t} = \hat{\mathcal{H}}(t) \Psi(k_0, t), \quad (\text{A8})$$

with  $\Psi(k_0, t) = \sum_{m=\text{CB, VB}} \beta^{(m)}(k_0, t) \Phi(k_0)$  being the electron wave function, where  $\Phi$  is the Bloch states of the field-free system and  $\beta^{(m)}$  is the expansion coefficients of Eq. (A8) [62].

## 3. Keldysh adiabaticity parameter

The general form of the Keldysh parameter for a two-band model reads

$$\gamma = \frac{\omega \sqrt{m^* \Delta}}{e E_0}, \quad (\text{A9})$$

where  $m^*$  is the effective electron mass [40]. Using Eqs. (A3) and (A5) we obtain

$$m^* = \hbar^2 \left[ \frac{\partial^2 \varepsilon(k)}{\partial k^2} \Big|_{k_0=0} \right]^{-1} = \frac{\Delta}{4v_F^2}. \quad (\text{A10})$$

Applying the Rabi frequency [Eq. (A7)], we rewrite the Keldysh adiabaticity parameter for an oscillating electric field as

$$\gamma = \frac{\omega \Delta}{2v_F e E_0} = \frac{\Delta}{2\hbar \Omega_R}. \quad (\text{A11})$$

Here, the Keldysh adiabaticity parameter is given as the characteristic interaction strength  $2\hbar \Omega_R$  and the band gap  $\Delta$ . Note that in the case of resonant excitation  $\hbar \omega = \Delta$  and  $\omega \ll \Omega_R$ , this regime is known as carrier-wave Rabi flopping.

## 4. Landau-Zener transition

Following the framework of Landau-Zener (LZ) transitions, it is useful to work with a Hamiltonian  $\hat{\mathcal{H}}'(t)$  with time-dependent diagonal components, which can be achieved by applying the unitary transformation

$$\hat{U} = \exp\left(i\frac{\pi}{4}\hat{\sigma}_y\right). \quad (\text{A12})$$

We obtain

$$\begin{aligned} \hat{\mathcal{H}}'(t) &= \hat{U} \hat{\mathcal{H}}(t) \hat{U}^{-1} \\ &= -\frac{\Delta}{2} \hat{\sigma}_x - \frac{\alpha}{2} \hat{\sigma}_z. \end{aligned} \quad (\text{A13})$$

In the vicinity of an LZ transition we linearize  $\alpha(t)$ , i.e.,  $\frac{\cos(\omega t)}{\omega} \approx t$  and obtain  $\alpha(t) \approx \alpha_0 t$ , with  $\alpha_0 = 2v_F e E_0$ . Now,  $\hat{\mathcal{H}}'(t)$  reads

$$\hat{\mathcal{H}}'(t) = -\frac{1}{2} \begin{pmatrix} \alpha_0 t & \Delta \\ \Delta & -\alpha_0 t \end{pmatrix}. \quad (\text{A14})$$

This Hamiltonian has the form of a Hamiltonian for an avoided crossing model with the Landau-Zener transition probability

$$P_{\text{LZ}} = \exp(-2\pi \delta_{\text{LZ}}), \quad (\text{A15})$$

with  $\delta_{\text{LZ}} = \Delta^2 / (4\hbar \alpha_0)$  being the Landau-Zener adiabaticity parameter [28]. For  $\delta_{\text{LZ}} \ll 1$ ,  $P_{\text{LZ}} \rightarrow 1$  and an interband transition becomes likely:

$$\delta_{\text{LZ}} = \frac{1}{4} \gamma \left( \frac{\hbar \omega}{\Delta} \right)^{-1} = \frac{\Delta^2}{8\hbar^2 \Omega_R \omega}. \quad (\text{A16})$$

## 5. Analytic resonance condition

When an electric field is applied to solids, the wave number  $k(t)$  of an electron changes according to Eq. (A4). Within one optical cycle, the resulting intraband motion leads to the accumulation of a dynamical phase,

$$\phi = \frac{1}{\hbar} \int_0^{T_0} \varepsilon(t) dt, \quad (\text{A17})$$

with  $T_0 = 2\pi/\omega$ . We assume a periodically oscillating electric field to obtain an analytic expression for the resonance condition under the presence of intraband motion. Using the Keldysh parameter, we rewrite Eq. (A3) as

$$\begin{aligned} \varepsilon(t) &= \sqrt{\Delta^2 + \left(2v_F \frac{E_0}{\omega} \cos(\omega t)\right)^2} \\ &= \Delta \sqrt{1 + \left(\frac{\cos(\omega t)}{\gamma}\right)^2}. \end{aligned} \quad (\text{A18})$$

Taking  $\omega t = t'$  and  $t'' = t' - \frac{\pi}{2}$ , we write

$$\begin{aligned} \phi &= \frac{2\Delta}{\hbar \omega} \int_0^\pi \sqrt{1 + \gamma^{-2} \cos(t')^2} dt' \\ &= \frac{4\Delta}{\hbar \omega} \int_0^{\frac{\pi}{2}} \sqrt{1 + \gamma^{-2} \sin(t'')^2} dt''. \end{aligned} \quad (\text{A19})$$

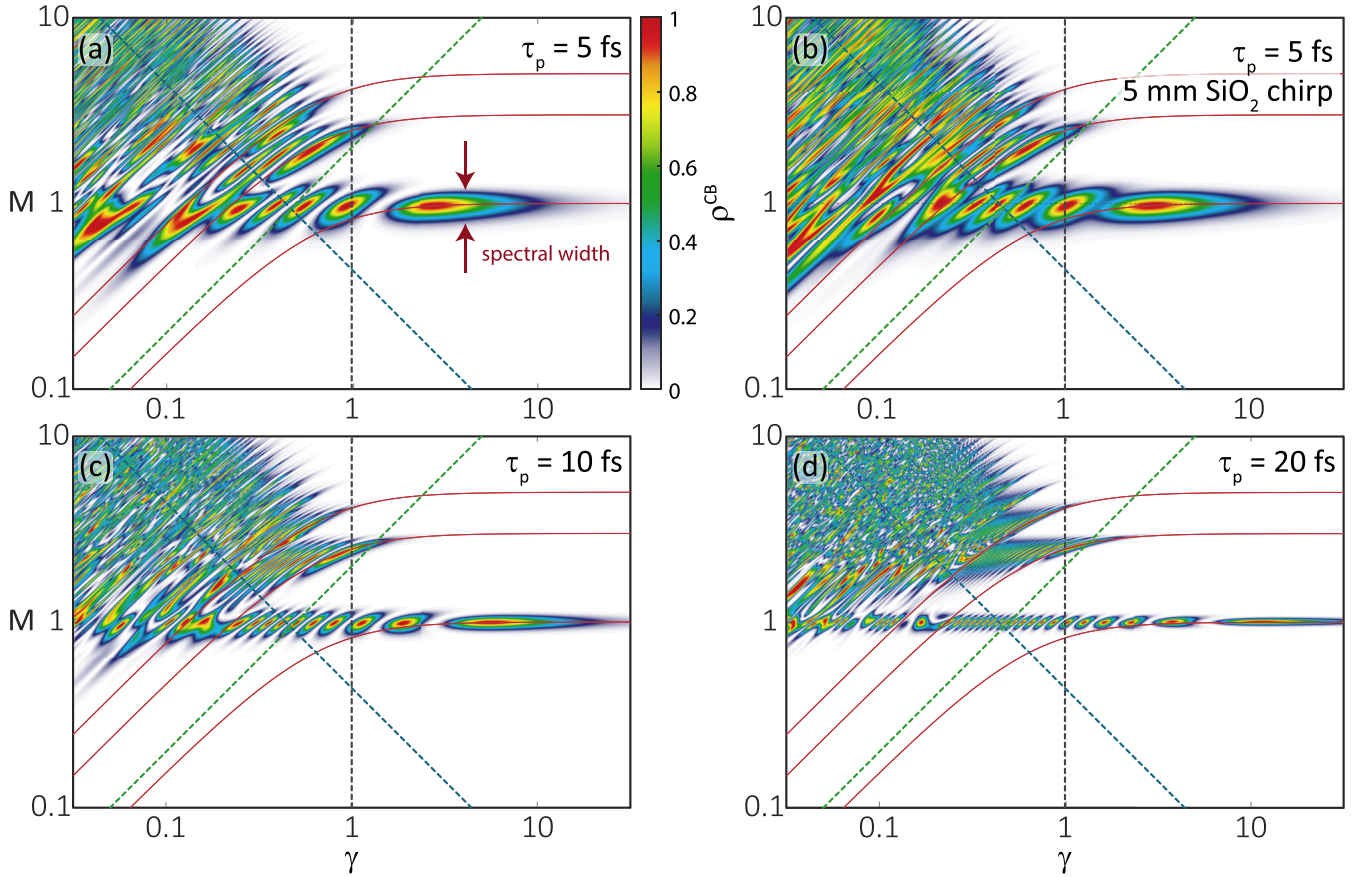


FIG. 5. Different pulse durations and dispersion. Map of the residual conduction band population for three different bandwidth-limited pulse durations [5 fs (a), 10 fs (c), 20 fs (d)] and for a 5-fs pulse with dispersion of 5 mm SiO<sub>2</sub> (b). Whereas for  $\gamma > 1$  only perturbative, resonant one-photon ( $n = 1$ ) absorption at  $M = 1$  is found, for  $\gamma < 1$  off-resonant excitation occurs. In particular, for  $P_{LZ} \approx 0.5$ ,  $\delta_{LZ} \approx \ln(2)/(2\pi)$ , and  $z_{\mathcal{R}} > 1$ , defining the adiabatic-impulsive regime, most off-resonant excitation is found. The red lines represent odd resonances for the light-matter interaction. The dashed green line represents  $z_{\mathcal{R}} = 1$  and the dashed blue line represents  $P_{LZ} \approx 0.5$ . See main text for detailed discussion.

Now we apply the complete elliptic integral of the second kind [63]:

$$\phi = \frac{4\Delta}{\hbar\omega} \mathbf{e}_l(-\gamma^{-2}). \quad (\text{A20})$$

When a phase of  $\phi = 2\pi$  is accumulated, the population at the next higher multiphoton resonance ( $n$ ) is found. Thus,

$$\frac{4\Delta}{\hbar\omega} \mathbf{e}_l(-\gamma^{-2}) \stackrel{!}{=} 2\pi n \quad (\text{A21})$$

needs to be fulfilled and the condition for analytical resonance under the presence of intraband motion reads

$$M = \frac{\pi n}{2\mathbf{e}_l(-\gamma^{-2})}. \quad (\text{A22})$$

For  $\gamma \gg 1$ , the elliptic integral becomes  $\frac{\pi}{2}$  and the photon resonances are found at multiples of the band gap ( $M = n$ ).

### 6. Genericity under pulse distortion and dephasing

The categorization of excitation regimes in a strongly driven two-band model is general and remains valid for different pulse durations, dispersion, and dephasing; i.e.,  $z_{\mathcal{R}}$ ,  $\delta_{LZ}$ , and  $\gamma$  depend on the driving frequency, the peak electric

field strength, and the energy spacing between the two bands. To prove this, we show in Fig. 5 the residual conduction band population for three different bandwidth-limited pulse durations [Fig. 5(a), 5 fs; Fig. 5(b), 10 fs; Fig. 5(c), 20 fs] centered at a photon energy of  $\hbar\omega = 1.55$  eV. Increasing the pulse duration results in a decrease in the spectral width of the photon orders and an increase of Rabi cycles as a function of  $\gamma$ , i.e., more Rabi cycles can be performed during the laser pulse. In the field-driven regimes, increasing the number of optical cycles results in more subsequent LZ transitions and a different accumulated dynamical phase. In the adiabatic-impulsive LZS regime, both lead to strong mixing of states, resulting in finer features in the residual conduction band population. Whereas the exact value of  $\rho^{\text{CB}}$  depends on the pulse shape, the categorization into different excitation regimes is determined by peak electric field strength.

Similarly, introducing dispersion does not affect the categorization. In Fig. 5(b) we show the residual conduction band population of the same pulse applied in Fig. 5(a), but stretched by 5 mm SiO<sub>2</sub> (Group delay dispersion: 180.8 fs<sup>2</sup>; Third-order dispersion, 137.3 fs<sup>3</sup>). The visibility of the Rabi oscillations is decreased since the spectral components are delayed with respect to each other. In

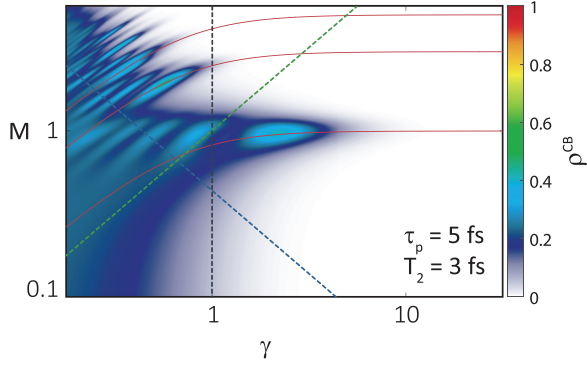


FIG. 6. Dephasing of the population. Map of the residual conduction band population assuming a dephasing time constant of  $T_2 = 3$  fs and a pulse duration of 5 fs. The red lines represent odd resonances for the light-matter interaction. The dashed green line represents  $z_{\mathcal{R}} = 1$  and the dashed blue line represents  $P_{LZ} \approx 0.5$ . See main text for detailed discussion.

the field-driven regimes, all features are preserved while, again, the exact value of the conduction band population is changed due to different accumulation of dynamical phase.

Figure 6 shows the residual conduction band population for a pulse duration of 5 fs including a dephasing time constant of  $T_2 = 3$  fs [25]. Decreasing the dephasing time results in an increase of  $\rho^{\text{CB}}$  in the adiabatic regime; i.e., transiently populated carriers remain after the laser pulse and the residual population in the adiabatic-impulsive LZS regime becomes smeared out. LZS interference becomes less important due to decoherence and the visibility of features decreases consequently. We note that the dephasing time constant  $T_2$  can be understood as decay of quantum coherence in a coherently driven system.

### 7. Relativistic regime

The classical equation of motion of a free electron in an optical field is given by

$$\frac{d\mathbf{p}}{dt} = -e[\mathbf{E}(\mathbf{x}, t) + \mathbf{v} \times \mathbf{B}(\mathbf{x}, t)], \quad (\text{A23})$$

with peak magnetic field  $|B_0| = E_0/c$  ( $c$ , speed of light;  $e$ , electron charge;  $\mathbf{p}$ , electron momentum;  $\mathbf{v}$ , electron velocity).

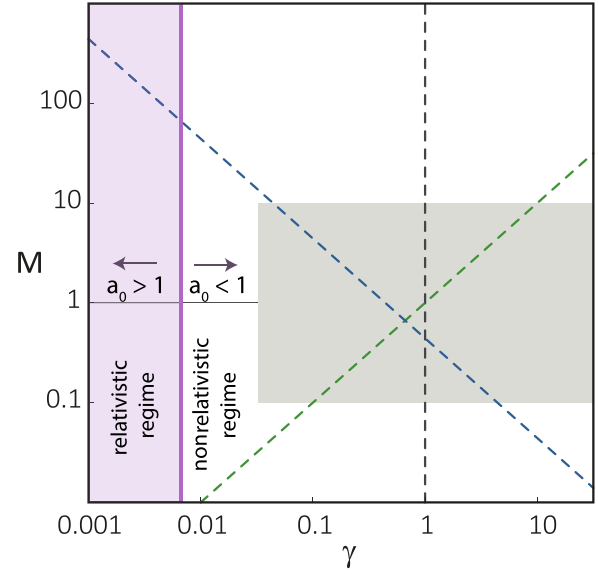


FIG. 7. Relativistic regime in the strongly driven TBS. The gray box represents the regimes discussed in this paper. Relativistic effects become important when the normalized vector potential  $a_0$  becomes smaller than 1. In the TBS system considered here, a Keldysh parameter smaller than 0.007 is required to enter the relativistic regime.

In classical Newtonian mechanics we assume that  $v \ll c$ . This implies that the contribution of the second term in Eq. (A23) is negligible. Assuming an oscillating electric field, the maximal velocity is  $v_{\text{max}} = eE_0/(\omega m_e)$ . When  $v_{\text{max}}$  becomes comparable to  $c$ , the normalized vector potential

$$a_0 = \frac{eE_0}{\omega m_e c} \quad (\text{A24})$$

reaches unity and relativistic effects become important [64]. In the case of a TBS, we replace the electron rest mass  $m_e$  with the effective mass [Eq. (A10)] and obtain

$$a_{0,\text{TBS}} = \frac{v_F}{\gamma c}. \quad (\text{A25})$$

The relativistic regime ( $a_0 > 1$ ) is entered for  $\gamma < \frac{v_F}{c}$ . Hence, in the TBS considered here with  $v_F = 1$  nm/fs, the magnetic component of the optical field can be neglected for  $\gamma > 0.007$ . Figure 7 shows the full  $\gamma$ - $M$  map including the relativistic regime.

- [1] P. Corkum and F. Krausz, *Nat. Phys.* **3**, 381 (2007).  
 [2] S. Ghimire and D. A. Reis, *Nat. Phys.* **15**, 10 (2019).  
 [3] G. Vampa, T. J. Hammond, N. Thiré, B. E. Schmidt, F. Légaré, C. R. McDonald, T. Brabec, and P. B. Corkum, *Nature (London)* **522**, 462 (2015).  
 [4] P. Jürgens, B. Liewehr, B. Kruse, C. Peltz, D. Engel, A. Husakou, T. Witting, M. Ivanov, M. J. Vrakking, T. Fennel, and A. Mermillod-Blondin, *Nat. Phys.* **16**, 1035 (2020).  
 [5] M. F. Ciappina, J. A. Pérez-Hernández, A. S. Landsman, W. A. Okell, S. Zherebtsov, B. Förg, J. Schötz, L. Seiffert, T. Fennel,

- T. Shaaran, T. Zimmermann, A. Chacón, R. Guichard, A. Zaïr, J. Tisch, J. Marangos, T. Witting, B. A., S. Maier, L. Roso *et al.*, *Rep. Prog. Phys.* **80**, 054401 (2017).  
 [6] A. Schiffrin, T. Paasch-Colberg, N. Karpowicz, V. Apalkov, D. Gerster, S. Mühlbrandt, M. Korbman, J. Reichert, M. Schultze, S. Holzner, J. V. Barth, R. Kienberger, R. Ernstorfer, V. S. Yakovlev, M. I. Stockman, and F. Krausz, *Nature (London)* **493**, 70 (2013).  
 [7] H. K. Kelardeh, V. Apalkov, and M. I. Stockman, *Phys. Rev. B* **91**, 045439 (2015).



- [8] T. Higuchi, C. Heide, K. Ullmann, H. B. Weber, and P. Hommelhoff, *Nature (London)* **550**, 224 (2017).
- [9] H. Liu, Y. Li, Y. S. You, S. Ghimire, T. F. Heinz, and D. A. Reis, *Nat. Phys.* **13**, 262 (2017).
- [10] C. Heide, T. Higuchi, H. B. Weber, and P. Hommelhoff, *Phys. Rev. Lett.* **121**, 207401 (2018).
- [11] N. Yoshikawa, T. Tamaya, and K. Tanaka, *Science* **356**, 736 (2017).
- [12] N. Yoshikawa, K. Nagai, K. Uchida, Y. Takaguchi, S. Sasaki, Y. Miyata, and K. Tanaka, *Nat. Commun.* **10**, 3709 (2019).
- [13] C. Heide, T. Boolakee, T. Higuchi, H. B. Weber, and P. Hommelhoff, *New J. Phys.* **21**, 045003 (2019).
- [14] C. Heide, T. Boolakee, T. Eckstein, and P. Hommelhoff, *Nanophotonics* 20210236 (2021).
- [15] C. Heide, T. Boolakee, T. Eckstein, C. Gerner, H. B. Weber, I. Franco, and P. Hommelhoff, [arXiv:2107.06848](https://arxiv.org/abs/2107.06848).
- [16] J. Reimann, S. Schlauderer, C. P. Schmid, F. Langer, S. Baierl, K. A. Kokh, O. E. Tereshchenko, A. Kimura, C. Lange, J. Güdde, U. Höfer, and R. Huber, *Nature (London)* **562**, 396 (2018).
- [17] S. Azar Oliaei Motlagh, F. Nematollahi, V. Apalkov, M. I. Stockman, S. A. Oliaei Motlagh, F. Nematollahi, V. Apalkov, M. I. Stockman, S. Azar Oliaei Motlagh, F. Nematollahi, V. Apalkov, and M. I. Stockman, *Phys. Rev. B* **100**, 115431 (2019).
- [18] C. Vaswani, L.-L. Wang, D. H. Mudiyansele, Q. Li, P. M. Lozano, G. D. Gu, D. Cheng, B. Song, L. Luo, R. H. J. Kim, C. Huang, Z. Liu, M. Mootz, I. E. Perakis, Y. Yao, K. M. Ho, and J. Wang, *Phys. Rev. X* **10**, 021013 (2020).
- [19] W. Nie, Z. H. Peng, F. Nori, and Y. X. Liu, *Phys. Rev. Lett.* **124**, 023603 (2020).
- [20] M. S. Mrudul, Á. Jiménez-Galán, M. Ivanov, and G. Dixit, *Optica* **8**, 422 (2020).
- [21] Y. Bai, F. Fei, S. Wang *et al.*, *Nat. Phys.* **17**, 311 (2021).
- [22] C. P. Schmid, L. Weigl, P. Grössing, V. Junk, C. Gorini, S. Schlauderer, S. Ito, M. Meierhofer, N. Hofmann, D. Afanasiev, J. Crewse, K. A. Kokh, O. E. Tereshchenko, J. Güdde, F. Evers, J. Wilhelm, K. Richter, U. Höfer, and R. Huber, *Nature (London)* **593**, 385 (2021).
- [23] L. Allen and J. H. Eberly, *Optical Resonance and Two-Level Atoms* (Dover, New York, 1987).
- [24] C. Cohen-Tannoudji, J. Dupont-Roc, and G. Grynberg, *Atom-Photon Interactions: Basic Processes and Applications* (Wiley, New York, 1998).
- [25] M. S. Wismer, S. Y. Kruchinin, M. Ciappina, M. I. Stockman, and V. S. Yakovlev, *Phys. Rev. Lett.* **116**, 197401 (2016).
- [26] S. Ashhab, J. R. Johansson, A. M. Zagorskin, and F. Nori, *Phys. Rev. A* **75**, 063414 (2007).
- [27] K. L. Ishikawa, *Phys. Rev. B* **82**, 201402(R) (2010).
- [28] S. N. Shevchenko, S. Ashhab, and F. Nori, *Phys. Rep.* **492**, 1 (2010).
- [29] L. A. Chizhova, F. Libisch, and J. Burgdörfer, *Phys. Rev. B* **94**, 075412 (2016).
- [30] F. Fillion-Gourdeau, D. Gagnon, C. Lefebvre, and S. MacLean, *Phys. Rev. B* **94**, 125423 (2016).
- [31] S. Y. Kruchinin, F. Krausz, and V. S. Yakovlev, *Rev. Mod. Phys.* **90**, 021002 (2018).
- [32] S. A. Sato, M. Lucchini, M. Volkov, F. Schlaepfer, L. Gallmann, U. Keller, and A. Rubio, *Phys. Rev. B* **98**, 035202 (2018).
- [33] C. Heide, T. Boolakee, T. Higuchi, and P. Hommelhoff, *J. Phys.: Photonics* **2**, 024004 (2020).
- [34] Q. Z. Li, P. Elliott, J. K. Dewhurst, S. Sharma, and S. Shallcross, *Phys. Rev. B* **103**, L081102 (2021).
- [35] T. Higuchi, M. I. Stockman, and P. Hommelhoff, *Phys. Rev. Lett.* **113**, 213901 (2014).
- [36] T. T. Luu, M. Garg, S. Yu. Kruchinin, A. Moulet, M. T. Hassan, and E. Goulielmakis, *Nature (London)* **521**, 498 (2015).
- [37] N. Tancogne-Dejean, O. D. Mücke, F. X. Kärtner, and A. Rubio, *Nat. Commun.* **8**, 745 (2017).
- [38] T. T. Luu, Z. Yin, A. Jain, T. Gaumnitz, Y. Pertot, J. Ma, and H. J. Wörner, *Nat. Commun.* **9**, 3723 (2018).
- [39] K. Kaneshima, Y. Shinohara, K. Takeuchi, N. Ishii, K. Imasaka, T. Kaji, S. Ashihara, K. L. Ishikawa, and J. Itatani, *Phys. Rev. Lett.* **120**, 243903 (2018).
- [40] L. V. Keldysh, *Sov. Phys. JETP* **20**, 1307 (1965).
- [41] H. R. Reiss, *Phys. Rev. A* **22**, 1786 (1980).
- [42] M. Wegener, *Extreme Nonlinear Optics* (Springer, Berlin, 2005).
- [43] L. D. Landau, *Phys. Z. Sowjetunion* **2**, 46 (1932).
- [44] C. Zener, *Proc. R. Soc. London, Ser. A* **137**, 696 (1932).
- [45] Y. Kayanuma, *Phys. Rev. A* **55**, R2495(R) (1997).
- [46] F. Bloch, *Z. Phys.* **52**, 555 (1929).
- [47] L. A. Chizhova, F. Libisch, and J. Burgdörfer, *Phys. Rev. B* **95**, 085436 (2017).
- [48] J. R. Rubbmark, M. M. Kash, M. G. Littman, and D. Kleppner, *Phys. Rev. A* **23**, 3107 (1981).
- [49] M. Shapiro, M. J. Vrakking, and A. Stolow, *J. Chem. Phys.* **110**, 2465 (1999).
- [50] G. Vampa, C. R. McDonald, G. Orlando, D. D. Klug, P. B. Corkum, and T. Brabec, *Phys. Rev. Lett.* **113**, 073901 (2014).
- [51] I. Franco and P. Brumer, *J. Phys. B: At., Mol. Opt. Phys.* **41**, 074003 (2008).
- [52] T. Boolakee, C. Heide, F. Wagner, C. Ott, M. Schlecht, J. Ristein, and H. B. Weber, *J. Phys. B: At., Mol. Opt. Phys.* **53**, 154001 (2020).
- [53] S. Ghimire, G. Ndabashimiye, A. D. Dichiaro, E. Sistrunk, M. I. Stockman, P. Agostini, L. F. Dimauro, and D. A. Reis, *J. Phys. B: At., Mol. Opt. Phys.* **47**, 204030 (2014).
- [54] M. Lezius, V. Blanchet, M. Y. Ivanov, and A. Stolow, *J. Chem. Phys.* **117**, 1575 (2002).
- [55] H. J. Wörner, J. B. Bertrand, B. Fabre, J. Higuier, H. Ruf, A. Dubrouil, S. Patchkovskii, M. Spanner, Y. Mairesse, V. Blanchet, E. Mével, E. Constant, P. B. Corkum, and D. M. Villeneuve, *Science* **334**, 208 (2011).
- [56] M. F. Kling, P. Von Den Hoff, I. Znakovskaya, and R. De Vivie-Riedle, *Phys. Chem. Chem. Phys.* **15**, 9448 (2013).
- [57] G. H. Wannier, *Phys. Rev.* **117**, 432 (1960).
- [58] A. F. Kockum, A. Miranowicz, S. De Liberato, S. Savasta, and F. Nori, *Nat. Rev. Phys.* **1**, 19 (2019).
- [59] P. Forn-Díaz, L. Lamata, E. Rico, J. Kono, and E. Solano, *Rev. Mod. Phys.* **91**, 025005 (2019).
- [60] B. Damski, *Phys. Rev. Lett.* **95**, 035701 (2005).
- [61] S. A. Oliaei Motlagh, J.-S. Wu, V. Apalkov, and M. I. Stockman, *Phys. Rev. B* **98**, 081406(R) (2018).

- [62] S. A. Oliaei Motlagh, F. Nematollahi, A. Mitra, A. J. Zafar, V. Apalkov, and M. I. Stockman, *J. Phys.: Condens. Matter* **32**, 065305 (2020).
- [63] M. Abramowitz, I. A. Stegun, and R. H. Romer, *Am. J. Phys.* **56**, 958 (1988).
- [64] M. Fuchs, R. Weingartner, A. Popp, Z. Major, S. Becker, J. Osterhoff, I. Cortrie, B. Zeitler, R. Hörlein, G. D. Tsakiris, U. Schramm, T. P. Rowlands-Rees, S. M. Hooker, D. Habs, F. Krausz, S. Karsch, and F. Grüner, *Nat. Phys.* **5**, 826 (2009).